

1 A Numerical Model of Cellular Blebbing:
2 A Volume-Conserving,
3 Fluid-Structure Interaction Model
4 of the Entire Cell

5 Jennifer Young¹, Sorin Mitran¹

6 ¹ University of North Carolina at Chapel Hill

Abstract

In animal cells, blebs are smooth, quasi-hemispherical protrusions of the plasma membrane that form when a section of the membrane detaches from the underlying actin cytoskeleton and is inflated by flowing cytosol. The mechanics behind this common cellular activity are not yet clear. As a first step in the development of a full computational framework, we present a numerical model of overall cell behavior based upon the interaction between a background Newtonian-fluid cytosol and elastic structures modeling the membrane and filaments. The detailed micromechanics of the cytoskeletal network are the subject of future work. Here, the myosin-driven contraction of the actin network is modeled through stressed elastic filaments. Quantitative models of cytoskeletal micromechanics and biochemistry require accurate estimates of local stress and flow conditions. The main contribution of this paper is the development of a computationally efficient fluid-structure interaction model based on operator splitting, to furnish this data. Cytosol volume conservation, (as supported by experimental evidence), is enforced through an intermediate energy minimization step. Realistic bleb formation and retraction is observed from this model, offering an alternative formulation to positing complex continuum behavior of the cytoplasm (e.g. poroelastic model of [Charras et al., 2008]).

1 Introduction

In animal cells, a bleb is a fluid-filled protrusion that forms when the plasma membrane separates from the underlying actin cytoskeleton [Charras et al., 2005, Dai and Sheetz, 1999, Sheetz et al., 2006], and is pushed outward by pressure-driven cytosol [Albrecht-Buehler, 1982, Charras et al., 2005, Cunningham, 1995, Erickson and Trinkaus, 1976]. Blebbing occurs during apoptosis [Charras et al., 2005, Mills et al., 1998, Sheetz et al., 2006], mitosis [Albrecht-Buehler, 1982, Dai and Sheetz, 1999, Erickson and Trinkaus, 1976], and cell spreading and motility [Charras et al., 2005, Cunningham, 1995, Dai and Sheetz, 1999]. During bleb formation and retraction, the overall cellular volume remains constant [Albrecht-Buehler, 1982, Charras et al., 2005, Cunningham, 1995]. The biomechanical process behind the phenomenon is not yet completely understood. There are several topics under discussion in the literature [Charras, 2008], including how to characterize the cell's cytoskeleton. One viewpoint posits the actin cortex to be a continuous medium, either as a poroelastic material [Charras et al., 2008] or as a highly viscous fluid [Alt and Dembo, 1999]. The continuum hypothesis excludes consideration of anisotropic microdynamics taking place within the cytoskeleton [Yoon et al., 2008]. We present here an alternative modeling approach that couples the motion of a Newtonian fluid (the cytosol) with the deformation of elastic structures (the membrane and filaments). This volume conserving, fluid structure interaction model lays the groundwork for a full, micromechanical computation of cytoskeletal dynamics to be presented in future work.

39 A number of computational models have been made to simulate protrusive activities in cells. Bottino and
40 Fauci [Bottino and Fauci, 1998] used an immersed boundary method to model directed motion in crawling
41 cells. Alt and Dembo [Alt and Dembo, 1999] took a two-phase fluid approach to cell locomotion, treating
42 both the actin filament cortex and the cytosol as viscous fluids. A system of generalized Stokes equations
43 with Darcy’s law was used to model the fluid flow, including the transition between the two fluid phases.
44 With respect to previous work, our model includes additional features such as a volume constraint to ensure
45 accurate computation of fluid variables, the dynamic elastic stresses of the membrane, and a framework
46 conducive to a forthcoming micromechanics description of the cytoskeleton.

47 **1.1 Biological Background**

48 **1.1.1 Cellular Structures**

49 The cellular structures thought to be involved in bleb formation are the actin cytoskeleton, the cytosol, and
50 the plasma membrane. The actin cytoskeleton is the peripheral, mesh-like structure composed primarily
51 of cross-linked actin filaments which gives the cell its mechanical strength and shape [Alberts et al., 2002,
52 Boal, 2002]. Motor protein polymers, myosin II, can be found interlaced among the actin filaments and are
53 capable of producing contractile forces within the cytoskeleton [Alt and Dembo, 1999]. A typical cytoskeleton
54 contains 100,000-400,000 actin filaments [Boal, 2002, Cano et al., 1991], with each 8 *nm* thick fiber ranging
55 in length from 0.2-20 μm [Boal, 2002, Cano et al., 1991, Janmey et al.,].

56 The cytosol is the fluid within the cell [Boal, 2002, Bray, 2000]. It is comprised of water and dissolved
57 proteins [Bray, 2000] with a viscosity of 1.1-3.0 *cP* [Bicknese et al., 1993, Mastro et al., 1984]. The fluid
58 pressure inside the cell is normally 20-300 *Pa* higher with respect to that of the external ambient fluid
59 [Charras et al., 2008, Rand and Burton, 1964].

60 The plasma membrane is a 4-5 *nm* thick, semi-permeable lipid bilayer that encases the actin cortex and
61 cytoplasm [Alberts et al., 2002, Boal, 2002]. The plasma membrane can only stretch 2-5% of its area before
62 rupturing [Evans and Skalak, 1980, Morris and Homann, 2001, Sheetz et al., 2006]. However, a cell houses
63 extra membrane surface area in folds, ruffles, microvilli and internal vacuole-like dilations to accommo-
64 date possible shape changes [Dai and Sheetz, 1999, Erickson and Trinkaus, 1976, Evans and Yeung, 1989,
65 Herring et al., 1999, Schmid-Schönbein et al., 1980, Sheetz et al., 2006]. The plasma membrane and cy-
66 toskeletal filaments are attached together via interactions with transmembrane proteins often mediated
67 by adaptor proteins, as well as via interactions with lipids [Alberts et al., 2002].

68 **1.1.2 Blebs**

69 Once a segment of membrane and cytoskeleton have separated, blebs take 3-10 seconds to fully expand
70 [Albrecht-Buehler, 1982, Charras et al., 2005, Cunningham, 1995]. Their sizes range from 5 - 125 μm^3 (about
71 0.003% to 15% of the overall cell volume) [Albrecht-Buehler, 1982, Cunningham, 1995] but they can be larger
72 for cells undergoing apoptosis [Sheetz et al., 2006]. A bleb usually remains expanded for 10-20 seconds and
73 then slowly retracts for 30-60 seconds [Cunningham, 1995, Dai and Sheetz, 1999]. Retraction occurs due
74 to the formation and subsequent myosin-driven contraction of a new actin mesh on the inside rim of the
75 bleb [Charras et al., 2006, Keller and Eggli, 1998]. This new cortex is built from protein monomers recruited
76 from the fluid within the bleb [Charras et al., 2006].

77 The initial membrane-cytoskeleton detachment is hypothesized to be due to a myosin II-driven contrac-
78 tion within the actin mesh [Charras et al., 2006, Pullarkat, 2006], creating a force that breaks the adhe-
79 sive bonds. At the site of bleb formation the plasma membrane morphs smoothly [Cunningham, 1995,
80 Dai and Sheetz, 1999], unfurling local folds and invaginations to provide for this shape change [Dai et al., 1998,
81 Erickson and Trinkaus, 1976, Schmid-Schönbein et al., 1980, Sheetz et al., 2006].

82 The overall cellular volume remains constant during bleb formation and retraction [Albrecht-Buehler, 1982,
83 Charras et al., 2005, Cunningham, 1995]. This supports the hypothesis that it is an internal fluid-membrane
84 interaction driving bleb expansion [Albrecht-Buehler, 1982, Charras et al., 2005, Cunningham, 1995], and
85 excludes the possibility of external fluid flow moving across the membrane into the bleb [Cunningham, 1995].
86 Actin polymerization does not play a role in bleb formation [Cunningham, 1995]. There is visual evidence of
87 the lack of actin in growing blebs [Albrecht-Buehler, 1982, Charras et al., 2006]. Figure 1 lists the sequence
88 of assumptions utilized in this model.

89 **2 Model Development**

90 **2.1 Mathematical Equations**

91 We present here the equations for a two-dimensional model of bleb formation and retraction. A two-
92 dimensional model was chosen due to the protrusion's approximate radial symmetry.

93 **2.1.1 Actin Filaments**

94 The cytoskeleton is a complex structure composed of approximately 10^5 cross-linked filaments [Boal, 2002].
95 We are currently constructing a detailed micromechanical network description of the cytoskeleton to be

96 presented in future work. Here, we consider the average effect of the cytoskeleton upon the blebbing phe-
97 nomenon, which appears in the form of filament forces imposed on the membrane.

98 Due to their length scale and mechanical properties [Janmey et al.,], actin filaments are modeled as one-
99 dimensional, elastic strings. Their forces are computed via Hooke's Law and added as external forces to the
100 membrane equation. Two types of filament forces are present in this model: (1) Filament forces at the cell's
101 periphery that model the membrane-cytoskeleton attachments and (2) Retraction filament forces that occur
102 inside the bleb as a myosin-driven contractile force on the protruded membrane.

103 **2.1.2 Monomer Concentrations**

104 In accordance with experimental evidence, retraction occurs when protein monomers present in the cytosol
105 are polymerized into filamentous actin and myosin polymers to form a new cortex [Charras et al., 2006].
106 These protein subunits diffuse [Kolega and Taylor, 1993, Zicha et al., 2003] and are advected [Zicha et al., 2003]
107 into the bleb by the locally surrounding fluid. We include the motion of these protein molecules via advection-
108 diffusion equations:

$$q_t + uq_x + vq_y = \alpha(q_{xx} + q_{yy}) + \phi(q)$$

109 where q is the free monomer concentration, u and v are the local fluid velocities and α is the diffusion
110 coefficient (see Figure 3 for coefficient values). The term $\phi(q)$ represents the transition of monomers to the
111 polymer state or vice versa, depending on polymerization and depolymerization rates. In blebbing, $\phi(q)$ is
112 mainly a sink term representing the net loss of monomers that get transformed into filament form within
113 the protrusion.

114 **2.1.3 Plasma Membrane**

115 Though the plasma membrane can be described by a fluid model [Alberts et al., 2002], micromechanical
116 measurements by scanning force microscopy suggest that an elastic model with varying elasticity mod-
117 ulus is also valid [Künneke et al., 2004]. Similar to the filament case [Boal, 2002, Dai and Sheetz, 1999,
118 Nichol and Hutter, 1996, Rawicz et al., 2000], the lipid bilayer is represented as a one-dimensional elastic
119 string. The membrane typically contains ruffles and invaginations which are unfurled to allow for cellular pro-
120 trusions [Dai et al., 1998, Erickson and Trinkaus, 1976, Schmid-Schönbein et al., 1980, Sheetz et al., 2006].
121 The presence of folds is modded by a strain-dependent elasticity modulus. A wrinkled membrane segment
122 is modeled by a compressed spring with a low, positive elasticity modulus representing the energy required
123 to overcome small membrane bending moments ($\approx 10^{-19}J$ [Boal, 2002]). This allows for large membrane

124 displacements that create small material stress. Once the strain reaches zero this equates to the biological
 125 membrane being completely unfolded. As strain increases, the elasticity modulus increases by several orders
 126 of magnitude [Künneke et al., 2004] to represent the membrane’s resistance to stretching. Figure 1 shows a
 127 schematic of the membrane’s stress-strain curve.

128 The motion of the membrane is modeled with a damped wave equation with forces from fluid pressure,
 129 viscosity, and the filaments added as source terms. Pressure pushes outward on the membrane, so this force
 130 is written as $\Delta p \cdot \mathbf{n}$ where p is pressure and \mathbf{n} is the normal vector. The filament forces are computed
 131 from Hooke’s law. The viscous forces are computed from the viscous stress tensor \mathbf{T} that arises in the fluid
 132 equation. The membrane equation is:

$$\lambda \delta_{tt} = E \delta_{SS} + \Delta p \cdot \mathbf{n} - \sum k(\Delta S \cdot \mathbf{n} + \Delta S \cdot \mathbf{t}) + \eta(\mathbf{T} \cdot \mathbf{n} + \mathbf{T} \cdot \mathbf{t})$$

133 where δ is the two-dimensional displacement vector, S is arc length, t is time, λ is a linear mass density, E is
 134 the varying elasticity modulus, η is the fluid viscosity, k is the filament spring constant, ΔS is the filament
 135 length displacement from equilibrium and \mathbf{t} is the membrane tangent vector. This is the equation of motion
 136 for the membrane when it is attached to the cytoskeleton. For a detached segment of membrane the filament
 137 force term is zero.

138 2.1.4 Cytosol

139 Blebs form due to the flow of pressurized cytosol [Albrecht-Buehler, 1982, Charras et al., 2005, Cunningham, 1995,
 140 Erickson and Trinkaus, 1976]. The fluid found in expanding blebs is devoid of filament fragments [Charras et al., 2005],
 141 thus the cytosol is modeled as an incompressible Newtonian fluid. During blebbing the cytosol undergoes
 142 low Reynolds flow ($Re \approx 10^{-6}$) due to the cell’s small length scale. The Stokes equations is utilized to solve
 143 for the fluid motion:

$$\begin{aligned} -\nabla p + \eta \Delta \mathbf{u} &= 0 \\ \nabla \cdot \mathbf{u} &= 0 \end{aligned}$$

144 where \mathbf{u} is the velocity vector.

145 **2.2 Numerical Methods**

146 The numerical fluid-structure interaction problem is solved through the operator splitting approach outlined
147 in Figure 2. We have developed a publicly available software implementation based upon the Bearclaw
148 framework for solving time dependent partial differential equations (PDEs) [Mitran, 2001].

149 **2.2.1 Solution methods for the individual equations**

150 To solve the hyperbolic elasticity portion of the membrane equation and the advection part of the concen-
151 tration equations, we employ a wave propagation algorithm [LeVeque, 1997]. The diffusion component of
152 the concentration equations is solved with a Crank-Nicolson scheme. Source terms are incorporated into the
153 solution of each equation via a fractional step method. The Stokes equations are recast in a vorticity-stream
154 function formulation [Fletcher, 1988], and solved using a multigrid iterative scheme.

155 **2.2.2 Grid Generation**

156 The cell is discretized with a curvilinear grid that is mapped to a Cartesian grid upon which all numerical
157 procedures are carried out. A conformal, orthogonal grid allows for straightforward implementation of
158 the numerical methods. Such a grid can be generated given the current cell boundary by solving a set of
159 PDEs derived from the Euler-Lagrange variational principle [Jose and Saletan, 1998, Ryskin and Leal, 1983,
160 Zhang et al., 2006]. To make the grid truly orthogonal requires that the boundary points be allowed to “slide”
161 along the boundary curve to orient themselves in orthogonally favorable positions that satisfy the Riemann
162 mapping theorem [Bak and Newman, 1997]. This results in a non-linear problem. To avoid the complications
163 of a non-linear solve, we enforce orthogonality in the domain’s interior and use general curvilinear grid
164 mapping procedures to compute boundary conditions for the fluid equations.

165 **2.2.3 Volume Constraint**

166 Biological experiments show that the fluid volume remains constant during blebbing [Albrecht-Buehler, 1982,
167 Charras et al., 2005, Cunningham, 1995]. The operator splitting procedure employed in the simulation offers
168 economy in computation but does not necessarily conserve volume. At a constant temperature, fluid stresses
169 and volume are related, so any artificial changes in volume will cause an artificial change in fluid stress.
170 To fix this issue, at an intermediate step in time advancement after the membrane has been moved to a
171 new position, we apply Gauss’ principle of least constraint to obtain a corrected membrane configuration

172 [Papastavridis, 2002]. Using the idea of Lagrange multipliers, we wish to minimize the following function:

$$L(x_i, y_i, \lambda) = E(x_i, y_i) + \lambda(V(x_i, y_i) - c)$$

173 where λ is the Lagrange multiplier, V is the current cell volume, c is the cell's initial volume that we wish to
174 maintain, and x_i, y_i are the membrane coordinate points. The total energy E expended by the cell includes
175 the elastic energy of the membrane and the work done by fluid pressure and filaments on the membrane.
176 The solution to this minimization problem is found using a quasi-Newton method [Bertsekas, 1982].

177 **3 Results**

178 We present results for a model cell. Parameter values (see Figure 3) were chosen to be close to those found
179 in the literature but do not model a particular cell type or scenario. The model can handle arbitrary initial
180 membrane conformations and filament distributions. We chose a circular membrane with filaments equally
181 distributed across the cell as a test case.

182 **3.1 Model of Bleb Formation and Retraction**

183 At the start of the simulation, filaments are in an extended state, the membrane is compressed (wrinkled), and
184 the pressure inside the cell is positive. A small number of adjacent filaments are released from the membrane
185 in one area of the cell. During subsequent time steps, filaments at the edges of the freed membrane are released
186 at a constant velocity. This velocity represents the average speed of membrane-filament detachment based on
187 comparing the membrane-cytoskeleton adhesion energy [Sheetz, 2001] and the energy in the membrane at the
188 edge of the bleb. As the freed membrane expands driven by fluid pressure, it entrains fluid that transports
189 actin and myosin monomers into the bleb. At each time step, a percentage of these actin monomers are
190 removed from the fluid and added to newly forming retraction filaments. This percentage parameter is
191 determined from the difference in polymerization and depolymerization rates for an actin filament under the
192 given monomer concentration. A similar procedure is carried out for myosin. Once a base cortex has been
193 established, the retraction filaments become active, contractile springs within the model. These filaments
194 collectively produce an inward force on the membrane. Figures 4-7 show series of simulation time steps,
195 displaying different variables such as fluid velocity, pressure, free actin monomer concentration, and the
196 presence of filament forces.

197 Figure 8 displays a graph of the total contractile force generated within the bleb as a function of the bound

198 myosin concentration. Initially, there is no retraction force because the proteins have not yet built up
199 enough within the bleb to form a basic cortex. Once thresholds have been reached, the new network begins
200 to contract. As protein levels continue to increase, so does the total force. The variability in force seen later
201 in the graph can be attributed to the fluctuating balance between the decreasing forces needed to pull the
202 shrinking bleb inward versus the increasing amount of bound proteins.

203 3.2 Validation

204 The numerical implementation of the various equations of motion were individually validated by comparing
205 the results against known analytical solutions for simpler problems. The curvilinear grid mapping was also
206 tested to ensure that it produced reasonable grids for the fluid domain.

207 As a test of the volume constraint, conditions were created to induce bleb formation, and the program was
208 run with and without the volume conservation procedure. In both cases, the volume of the initial membrane
209 configuration was compared to the volume of the blebbed membrane. The results are displayed in Figure 9.
210 With no constraint there is clearly a decrease in volume, while in the volume constraint case although the
211 bleb forms, the rest of the membrane adjusts to maintain the overall cell volume.

212 As a general validation of the overall model, the code was run using three levels of fluid grid discretization:
213 12×12 , 24×24 and 48×48 . We compared the perimeter and area of a bleb at different points in time given
214 the same initial parameters for the three grids. The results are shown in Figure 10.

215 4 Discussion

216 We have developed an entire-cell, fluid-structure interaction model of cellular blebbing. It is a first step
217 in the construction of a continuum-microscopic framework, to be completed in subsequent work with a
218 micromechanical computation of the cytoskeleton. The complex actin cortex micromechanics are represented
219 here through average forces exerted through an equivalent elastic filament network. In the next stage of the
220 model, the micromechanical computation will be used to more accurately update these average forces at each
221 time step. We adopt a reductionist approach [Mogilner, 2009] in the construction of the computational model
222 in which separate components are modeled individually. Some biologically relevant conclusions can already be
223 drawn from the current computational model: (1) Bleb retraction is successfully predicted by the formation
224 of a new cytoskeleton built from actin and myosin subunits, using accepted values for protein diffusivity and
225 the computed advection velocity field. Also, the model simulates blebs of realistic geometric complexity. (2)

226 The model constitutes an alternative to invoking complex continuum behavior for the cytoskeleton immersed
227 in cytosol such as the poroelastic hypothesis of [Charras et al., 2008]. Localized in space and time stress
228 nonuniformities are obtained in the model. Furthermore, these nonuniformities can readily be linked to
229 detailed micromechanics of the cytoskeleton through the equivalent filament force concept introduced here.
230 In contrast, a complex, time-dependent constitutive law would be required in a poroelastic descriptions of
231 the cytoskeleton-cytosol ensemble. (3) The behavior of the membrane is realistically captured by a strain-
232 dependent elasticity modulus as supported by scanning-force microscopy data [Künneke et al., 2004]. Again,
233 this modeling approach can more readily be linked to microscopic computations of membrane dynamics
234 by comparison to a fluid mosaic model [Alberts et al., 2002]. (4) The volume constraint present in the
235 model ensures accurate computation of cytosol flow. In immersed interface or immersed boundary methods
236 [Bottino and Fauci, 1998], the distributed singularity techniques often lead to small numerical fluid fluxes
237 through the membrane which should be impermeable at the scale of the blebbing phenomenon. Though such
238 errors tend to cancel out globally and have little effect on overall quantities (e.g. bleb volume), they would
239 adversely affect local micromechanical and biochemical network descriptions like those we intend to add to
240 the model. The least constraint step used in the algorithm we present here ensures that accurate fluid stress
241 and velocity fields are obtained everywhere, even close to the membrane.

242 In the future, we plan to add more biological factors to the model such as levels of the membrane-cytoskeleton
243 adhesive proteins. We are currently working on including a micromechanics model of the cytoskeleton to
244 furnish the filament equivalent forces introduced in this model. The current work is a step in providing a
245 software platform to answer quantitative questions about blebbing, one of the current challenges in compu-
246 tational biology [Mogilner, 2009].

247 **Acknowledgments**

248 This project developed after discussions with Dr. Timothy Elston, Dr. Kenneth Jacobson, and Gabriel
249 Weinreb on modeling blebs. The research effort was partially supported by NIH grant R01-HL077546-
250 5401A2.

References

- 251
- 252 [Alberts et al., 2002] Alberts, B., Johnson, A., Lewis, J., Raff, M., Roberts, K., and Walter, P. (2002).
253 *Molecular biology of the cell*. Garland, fourth edition.
- 254 [Albrecht-Buehler, 1982] Albrecht-Buehler, G. (1982). Does blebbing reveal the convulsive flow of liquid
255 and solutes through the cytoplasmic meshwork? *Cold Spring Harbor Symposia on Quantitative Biology*,
256 46(1):45–49.
- 257 [Alt and Dembo, 1999] Alt, W. and Dembo, M. (1999). Cytoplasm dynamics and cell motion: two-phase
258 fluid models. *Mathematical Biosciences*, 156(1-2):207–228.
- 259 [Bak and Newman, 1997] Bak, J. and Newman, D. J. (1997). *Complex Analysis*. Springer-Verlag, second
260 edition.
- 261 [Bertsekas, 1982] Bertsekas, D. P. (1982). *Constrained optimization and Lagrange multiplier methods*. Aca-
262 demic Press.
- 263 [Bicknese et al., 1993] Bicknese, S., Periasamy, N., Shohet, S. B., and Verkman, A. S. (1993). Cytoplasmic
264 viscosity near the cell plasma membrane: measurement by evanescent field frequency-domain microflu-
265 orimetry. *Biophysical Journal*, 65(3):1272–1282.
- 266 [Boal, 2002] Boal, D. (2002). *Mechanics of the cell*. Cambridge University Press.
- 267 [Bottino and Fauci, 1998] Bottino, D. and Fauci, L. (1998). A computational model of ameboid deformation
268 and locomotion. *European Biophysics Journal*, 27(5):532–539.
- 269 [Bray, 2000] Bray, D. (2000). *Cell Movements: From Molecules to Motility*. Garland, second edition.
- 270 [Cano et al., 1991] Cano, M. L., Lauffenburger, D. A., and Zigmond, S. H. (1991). Kinetic analysis of f-
271 actin depolymerization in polymorphonuclear leukocyte lysates indicates that chemoattractant stimulation
272 increases actin filament number without altering the filament length distribution. *The Journal of Cell*
273 *Biology*, 115:677–687.
- 274 [Charras, 2008] Charras, G. T. (2008). A short history of blebbing. *Journal of Microscopy*, 231(3):466–478.
- 275 [Charras et al., 2008] Charras, G. T., Coughlin, M., Mitchison, T. J., and Mahadevan, L. (2008). Life and
276 times of a cellular bleb. *Biophysical Journal*, 94(5):1836–1853.
- 277 [Charras et al., 2006] Charras, G. T., Hu, C., Coughlin, M., and Mitchison, T. J. (2006). Reassembly of
278 contractile actin cortex in cell blebs. *The Journal of Cell Biology*, 175(3):477–490.
- 279 [Charras et al., 2005] Charras, G. T., Yarrow, J. C., Horton, M. A., Mahadevan, L., and Mitchison, T. J.
280 (2005). Non-equilibration of hydrostatic pressure in blebbing cells. *Nature*, 435:365–369.
- 281 [Cunningham, 1995] Cunningham, C. C. (1995). Actin polymerization and intracellular solvent flow in cell
282 surface blebbing. *The Journal of Cell Biology*, 129(6):1589–1599.
- 283 [Dai and Sheetz, 1999] Dai, J. and Sheetz, M. P. (1999). Membrane tether formation from blebbing cells.
284 *Biophysical Journal*, 77(6):3363–3370.
- 285 [Dai et al., 1998] Dai, J., Sheetz, M. P., Wan, X., and Morris, C. E. (1998). Membrane tension in swelling
286 and shrinking molluscan neurons. *The Journal of Neuroscience*, 18(17):6681–6692.
- 287 [Erickson and Trinkaus, 1976] Erickson, C. A. and Trinkaus, J. P. (1976). Microvilli and blebs as sources of
288 reserve surface membrane during cell spreading. *Experimental Cell Research*, 99(2):375–384.
- 289 [Evans and Skalak, 1980] Evans, E. and Skalak, R. (1980). *Mechanics and thermodynamics of biomembranes*.
290 CRC Press.

- 291 [Evans and Yeung, 1989] Evans, E. and Yeung, A. (1989). Apparent viscosity and cortical tension of blood
292 granulocytes determined by micropipet aspiration. *Biophysical Journal*, 56(1):151–160.
- 293 [Fletcher, 1988] Fletcher, C. A. J. (1988). *Computational techniques for fluid dynamics: Volume 2*. Springer-
294 Verlag, second edition.
- 295 [Herring et al., 1999] Herring, T. L., Cohan, C. S., Welnhof, E. A., Mills, L. R., and Morris, C. E. (1999).
296 F-actin at newly invaginated membrane in neurons: implications for surface area regulation. *Journal of*
297 *Membrane Biology*, 171(2):151–169.
- 298 [Janmey et al.,] Janmey, P. A., Tang, J. X., and Schmidt, C. F. Actin filaments (unpublished).
- 299 [Jose and Saletan, 1998] Jose, J. V. and Saletan, E. J. (1998). *Classical dynamics: A contemporary approach*.
300 Cambridge University Press.
- 301 [Keller and Egli, 1998] Keller, H. and Egli, P. (1998). Protrusive activity, cytoplasmic compartmentaliza-
302 tion, and restriction rings in locomoting blebbing walker carcinosarcoma cells are related to detachment
303 of cortical actin from the plasma membrane. *Cell Motility and the Cytoskeleton*, 41(2):181–193.
- 304 [Kolega and Taylor, 1993] Kolega, J. and Taylor, D. L. (1993). Gradients in the concentration and assembly
305 of myosin ii in living fibroblasts during locomotion and fiber transport. *Molecular Biology of the Cell*,
306 4(8):819–836.
- 307 [Künneke et al., 2004] Künneke, S., Krüger, D., and Janshoff, A. (2004). Scrutiny of the failure of lipid mem-
308 branes as a function of headgroups, chain length, and lamellarity measured by scanning force microscopy.
309 *Biophysical Journal*, 86(3):1545–1553.
- 310 [LeVeque, 1997] LeVeque, R. (1997). Wave propagation algorithms for multidimensional hyperbolic systems.
311 *Journal of Computational Physics*, 131:327–353.
- 312 [Mastro et al., 1984] Mastro, A. M., Babich, M. A., Taylor, W. D., and Keith, A. D. (1984). Diffusion of a
313 small molecule in the cytoplasm of mammalian cells. *Proceedings of the National Academy of Sciences of*
314 *the United States of America*, 81(11):3414–3418.
- 315 [Mills et al., 1998] Mills, J. C., Stone, N. L., Erhardt, J., and Pittman, R. N. (1998). Apoptotic membrane
316 blebbing is regulated by myosin light chain phosphorylation. *The Journal of Cell Biology*, 140(3):627–636.
- 317 [Mitran, 2001] Mitran, S. (2001). Bearclaw. <http://coanda.amath.unc.edu/bearclaw>.
- 318 [Mogilner, 2009] Mogilner, A. (2009). Mathematics of cell motility: have we got its number? *Journal of*
319 *Mathematical Biology*, 58(1-2):105–134.
- 320 [Morris and Homann, 2001] Morris, C. E. and Homann, U. (2001). Cell surface area regulation and mem-
321 brane tension. *The Journal of Membrane Biology*, 179(2):79–102.
- 322 [Nichol and Hutter, 1996] Nichol, J. A. and Hutter, O. F. (1996). Tensile strength and dilatational elasticity
323 of giant sarcolemmal vesicles shed from rabbit muscle. *The Journal of Physiology*, 493(1):187–198.
- 324 [Papastavridis, 2002] Papastavridis, J. G. (2002). *Analytical mechanics: A comprehensive treatise on the*
325 *dynamics of constrained systems; For engineers, physicists, and mathematicians*. Oxford University Press.
- 326 [Pullarkat, 2006] Pullarkat, P. A. (2006). Loss of cell-substrate adhesion leads to periodic shape oscillations
327 in fibroblasts. *eprint arXiv:physics/0612156*.
- 328 [Rand and Burton, 1964] Rand, R. P. and Burton, A. C. (1964). Mechanical properties of the red cell
329 membrane. i. membrane stiffness and intracellular pressure. *Biophysical Journal*, 4(2):115–135.
- 330 [Rawicz et al., 2000] Rawicz, W., Olbrich, K. C., McIntosh, T., Needham, D., and Evans, E. (2000). Effect
331 of chain length and unsaturation on elasticity of lipid bilayers. *Biophysical Journal*, 79(1):328–339.

- 332 [Ryskin and Leal, 1983] Ryskin, G. and Leal, L. G. (1983). Orthogonal mapping. *Journal of Computational*
333 *Physics*, 50:71–100.
- 334 [Schmid-Schönbein et al., 1980] Schmid-Schönbein, G. W., Shih, Y. Y., and Chien, S. (1980). Morphometry
335 of human leukocytes. *Blood*, 56(5):866–875.
- 336 [Sheetz, 2001] Sheetz, M. P. (2001). Cell control by membrane-cytoskeleton adhesion. *Nature Reviews.*
337 *Molecular Cell Biology*, 2(5):392–396.
- 338 [Sheetz et al., 2006] Sheetz, M. P., Sable, J. E., and Döbereiner, H. (2006). Continuous membrane-
339 cytoskeleton adhesion requires continuous accommodation to lipid and cytoskeleton dynamics. *Annual*
340 *Review of Biophysics and Biomolecular Structure*, 35:417–434.
- 341 [Yoon et al., 2008] Yoon, Y., Kotar, J., Yoon, G., and Cicuta, P. (2008). The nonlinear mechanical response
342 of the red blood cell. *Physical Biology*, 5(3):036007.
- 343 [Zhang et al., 2006] Zhang, Y., Jia, Y., and Wang, S. (2006). 2d nearly orthogonal mesh generation with
344 controls on distortion function. *Journal of Computational Physics*, 218(2):549–571.
- 345 [Zicha et al., 2003] Zicha, D., Dobbie, I. M., Holt, M. R., Monypenny, J., Soong, D. Y. H., Gray, C., and
346 Dunn., G. A. (2003). Rapid actin transport during cell protrusion. *Science*, 300(5616):142–145.

347 **Figure Captions**

348 **Figure 1:** Sequence of model assumptions for a blebbing scenario (left) and a schematic graph of the
349 stress-strain relationship of the plasma membrane (right).

350 **Figure 2:** The sequence of steps which occurs during one time step of the simulation.

351 **Figure 3:** List of parameter values used in the simulation.

352 **Figure 4 and 5:** A series of snapshots of the cell membrane as the bleb forms and retracts. The full
353 cell figures (left) show fluid velocity vectors, while the zoom view figures (right) depict either the pressure
354 contours or the free actin monomer concentration contours. Pressure values shown are the actual values
355 minus the initial uniform pressure of 103 Pa. Note that the pressure is slightly higher inside the bleb during
356 expansion, but drops to lower values during retraction. Also note that the free actin monomer concentration
357 (in mg/ml) decreases in the bleb over time as the monomers are converted to filamentous actin.

358 **Figure 6 and 7:** A series of zoom view snapshots of the membrane and filament forces as the bleb forms
359 and retracts. The filaments which appear in the later time steps within the bleb are there to represent the
360 forces generated by the newly forming and contracting actin cortex.

361 **Figure 8:** The total force generated by the retracting bleb cortex versus the bound myosin concentration
362 within the bleb.

363 **Figure 9:** In the left column, the dotted circles depicts the initial position of the membrane, while the solid
364 line represents the membrane at a later time once blebbing has begun. The top figure does not have a volume
365 constraint imposed, while the bottom one does. The two graphs to the right plot the relative error between
366 the radii of the blebbed membrane vs. the initial membrane with respect to position on the membrane. If
367 volume is being conserved, the integral of the graph should be close to zero, which it is for the bottom graph
368 but not for the top graph.

369 **Figure 10:** These graphs show the evolution of the perimeter (left) and area (right) of a bleb over time for
370 three grid discretizations using the same parameter set.

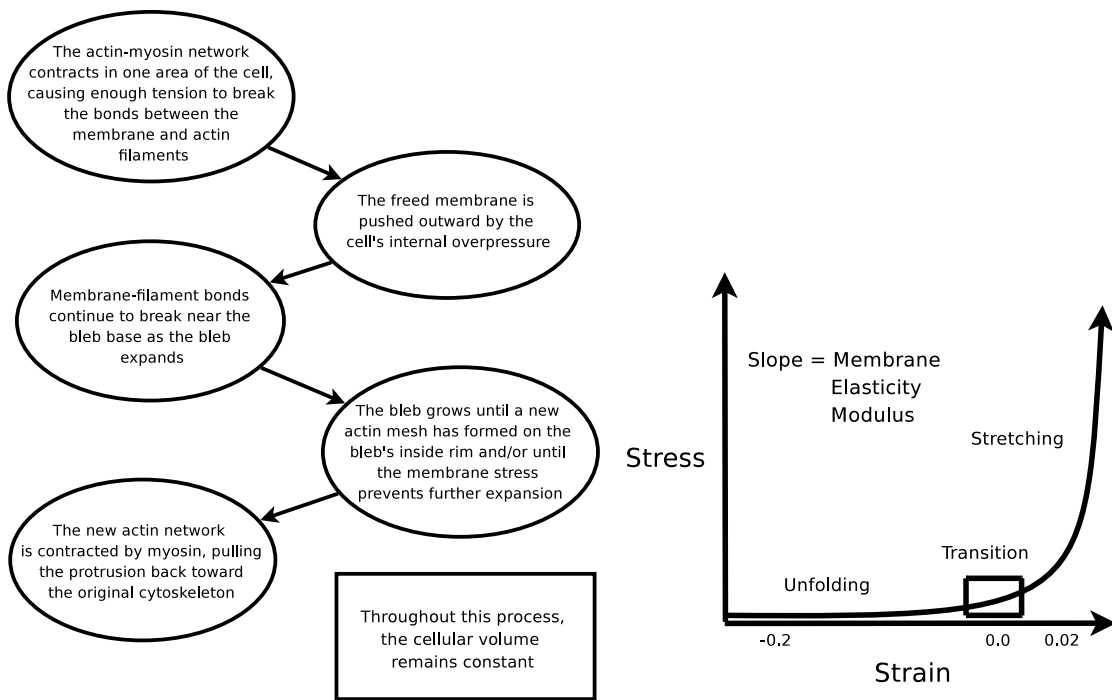


Figure 1:

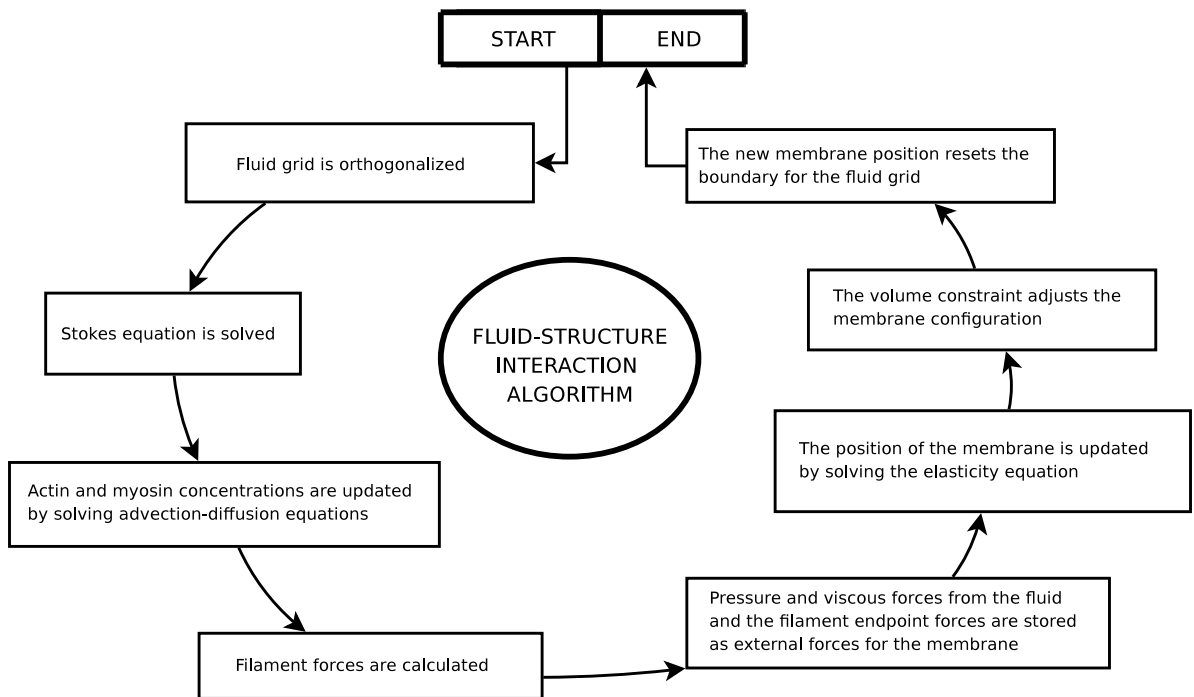


Figure 2:

Parameter	Value in SI units
Cell Diameter	10 μm
Regular Filament Equilibrium Length	3.4 μm
Regular Filament Strains	< 1%
Filament Spring Constant	20.5 pN/nm
Percentage of Excess Membrane	25%
Approximate Expansion Time	10 s
Approximate Stasis and Retraction Time	30 s
Total Number of Filaments in Model	1024
Filament/Membrane Detachment Rate	5 $filaments/s$
Bleb Diameter (fully expanded)	0.7 μm
Fluid Viscosity	1.3 cP
Pressure Difference across Membrane	103 Pa
Actin Diffusion Coefficient	$10^{-8} cm^2/s$
Myosin Diffusion Coefficient	$10^{-9} cm^2/s$

Figure 3:

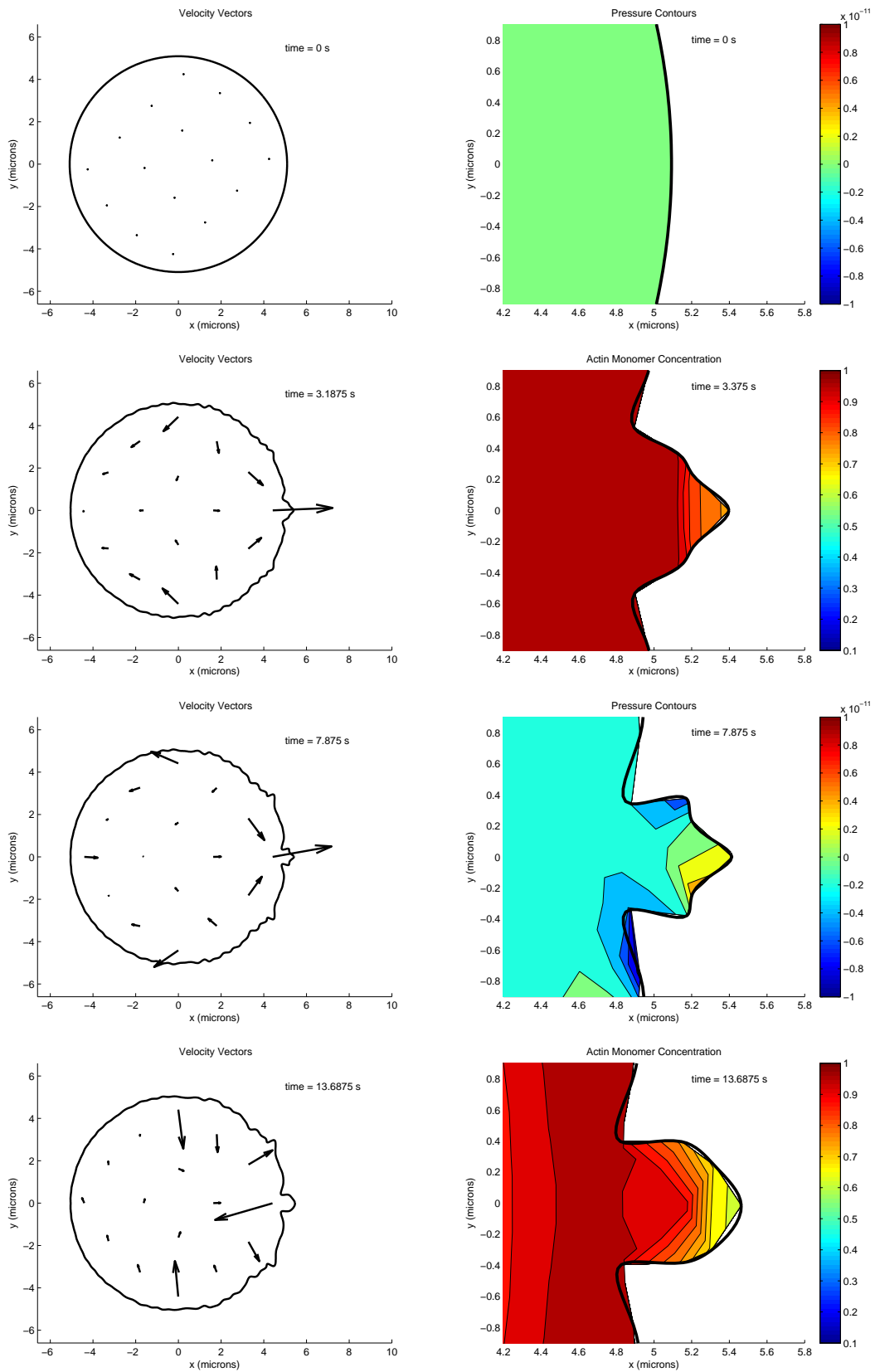


Figure 4:

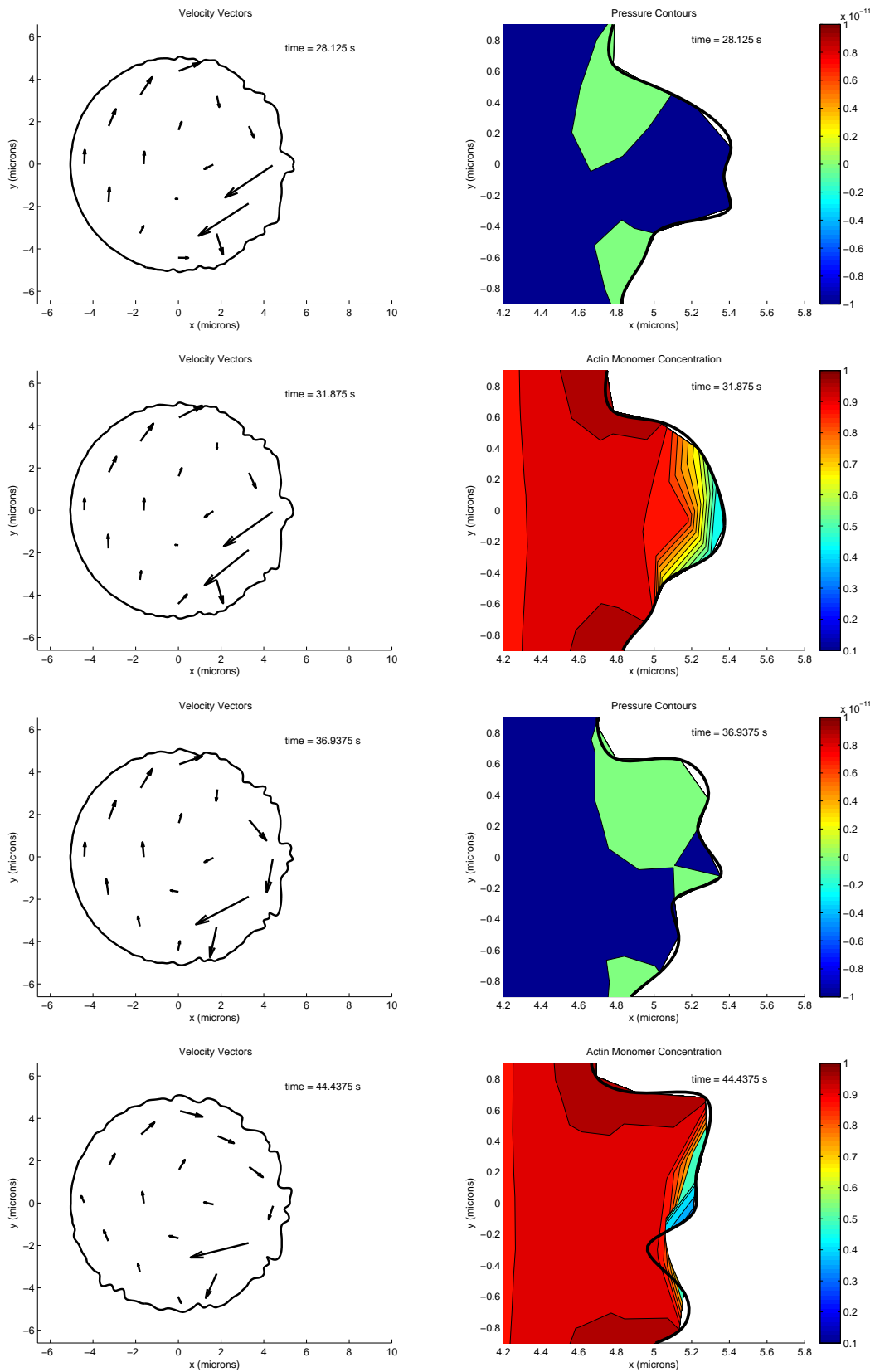


Figure 5:

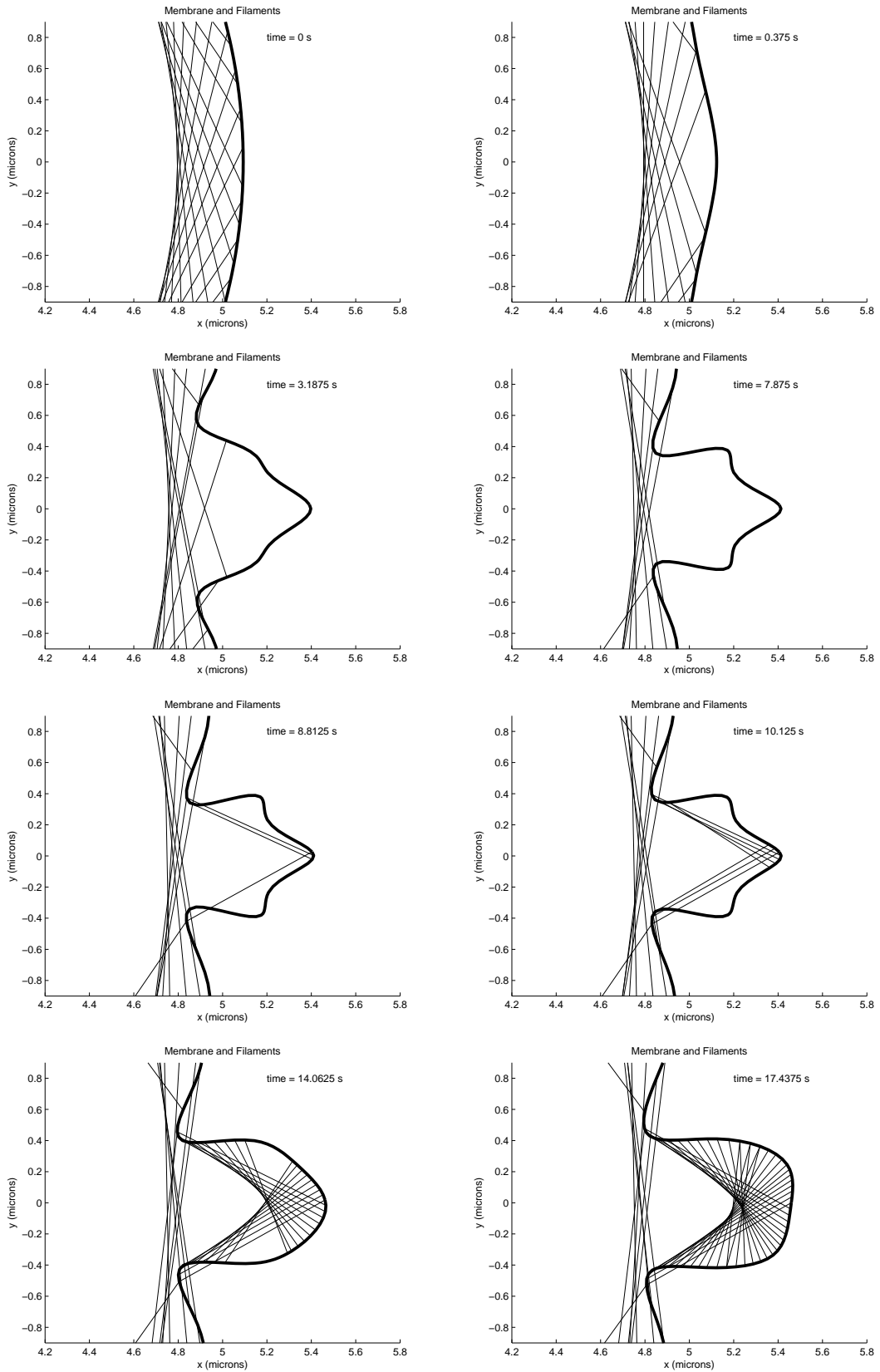


Figure 6:

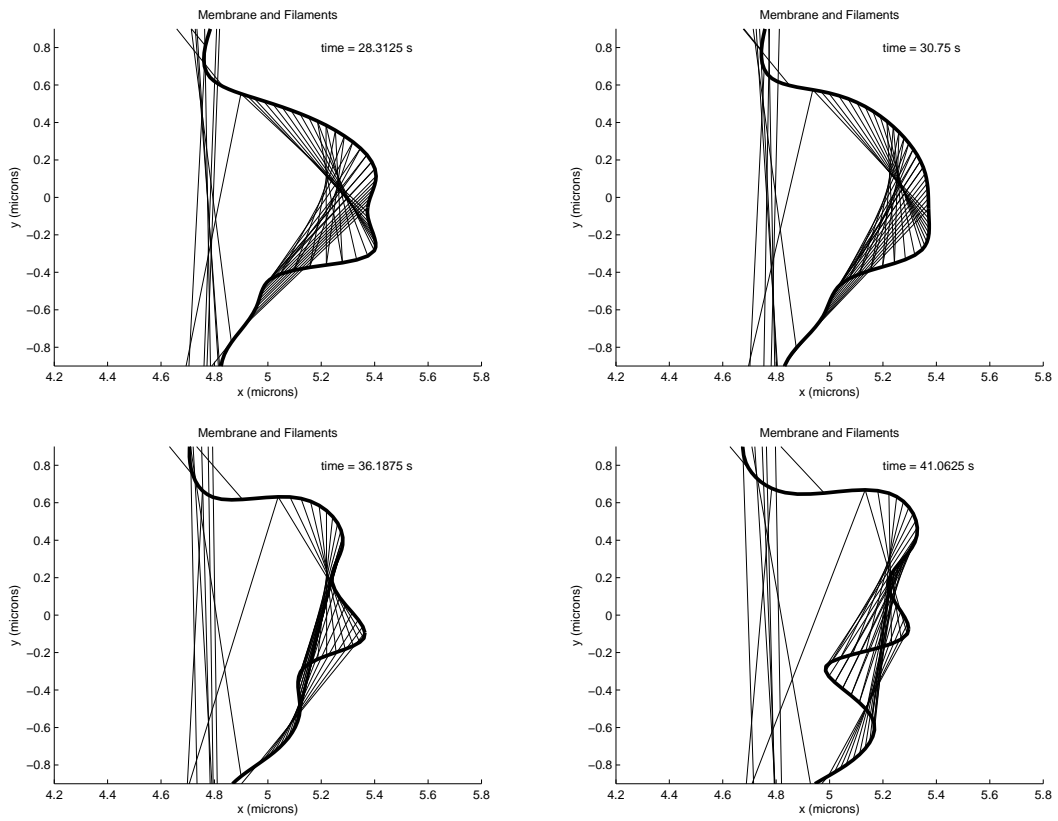


Figure 7:

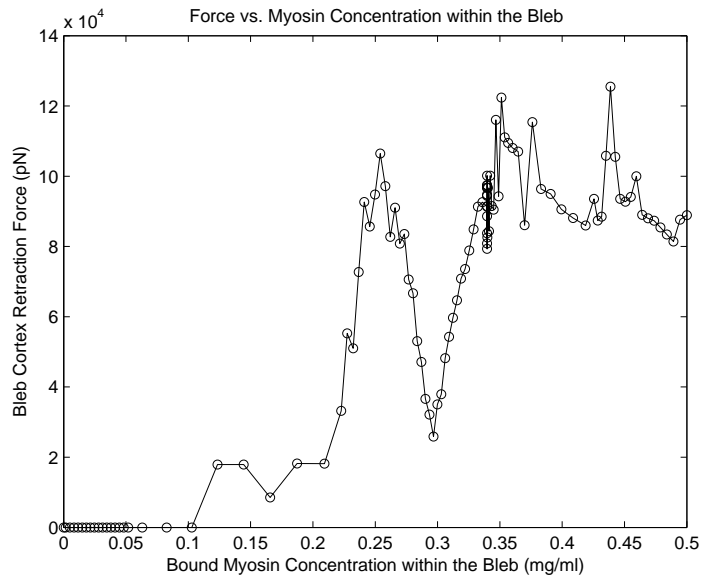


Figure 8:

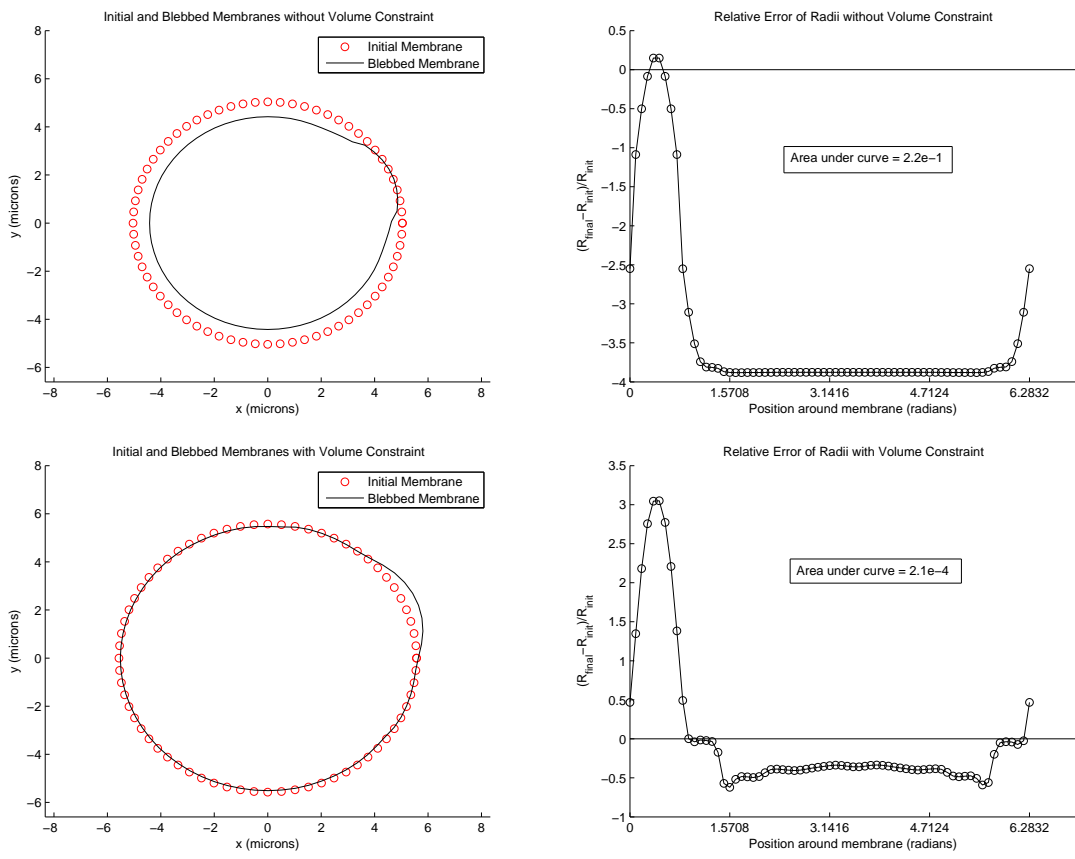


Figure 9:

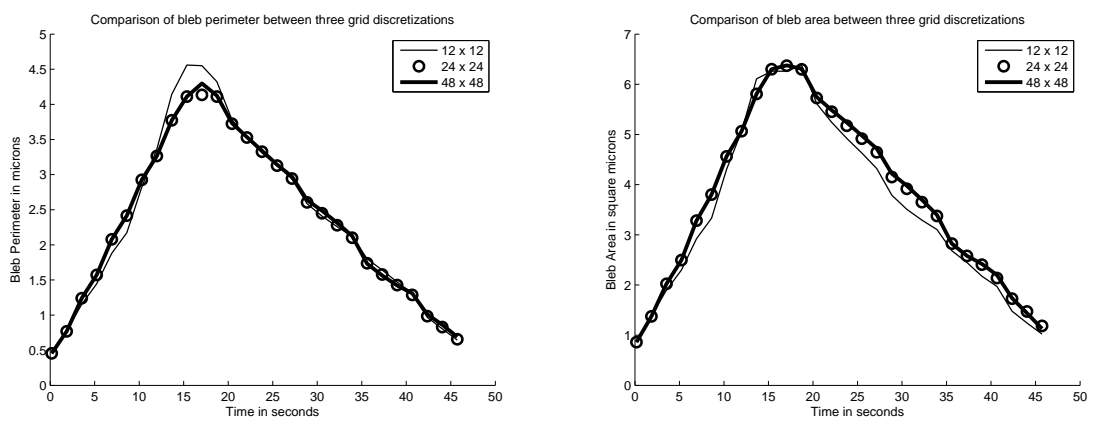


Figure 10: